ELSEVIER

International Journal of Heat and Fluid Flow 23 (2002) 366–372

International Journal of HEAT AND FLUID FLOW

www.elsevier.com/locate/ijhff

Natural convection in a vertical rectangular enclosure with symmetrically localized heating and cooling zones ☆

I. Ishihara *, T. Fukui, R. Matsumoto

Department of Mechanical Engineering, Kansai University, 3-3-35 Yamate-cho, Suita, Osaka 564-8680, Japan

Abstract

Numerical and experimental studies of natural convection in a single-phase, closed thermosyphon were carried out, using a vertical, rectangular enclosure model. Two vertical plates, each 100×100 mm^2 in dimension, and placed symmetrically play the role of heat transfer surfaces. These symmetrical heat transfer surfaces are separated into three horizontal zones of equal height; the top and bottom thirds of these surfaces are the zones of, respectively, cooling and heating, the intermediate section being an adiabatic zone. Silicon oil is used as the working fluid. Variable parameters are the distance, D, between the two heat transfer surfaces, and temperature difference, ΔT, between the heating and cooling zones. By changing both D and ΔT, three regimes of natural convection flow; steady, quasi-two-dimensional, steady, three-dimensional, and unsteady flows were found in experiment. Converged solutions obtained by numerical simulation agreed well with experimental results with regard to the temperature and velocity of the fluid as visualized by means of thermo-sensitive liquid crystal powders.

1. Introduction

In this research, a vertical rectangular enclosure was used as test section in modeling a single-phase, closed thermosyphon. Much previous research related to natural convection in single-phase closed thermosyphon describes the fluid flow and heat transfer in a vertical circular pipe. In such a case, the variable parameters will be the aspect ratio of the diameter to the length of the pipe, the temperature difference between heat transfer surfaces, and the Prandtl number of the working fluid.

For instance, Bayley and Lock (1965) presumed that fluid flow might be classified into three regimes—a classification based on the difference in temperature between the heating and the cooling surfaces: namely, (1) in the case of a small temperature difference between the two, a weak convection flow takes place in each zone, each of these flows being independent of the flows in other zones; (2) with a large temperature difference, upward and downward flows will mutually interpenetrate their opposite zones, after colliding and mixing in the intermediate zone; and (3) where there is only a moderate temperature difference, there appears an impeded flow that is yet free of any similar collision between upward and downward flows.

Japikse (1973) illustrated the flow visualized at the cross-section in a circular thermosyphon filled with air. Detailed flow pattern in the cross-sections, however, and that for the whole region of the thermosyphon, both remain undefined.

Mallinson et al. (1981) made numerical and experimental studies of the three-dimensional flow and heat transfer effected by natural convection in a closed, rectangular thermosyphon without any adiabatic zone, and have reported detailed flow and temperature patterns.

The present authors, Ishihara et al. (2000), have previously performed a study similar to the present one, but using a vertical rectangular enclosure in which only one of the vertical walls acted as heat transfer surface. And fluid flow and thermal characteristics were revealed, both numerically and experimentally.

Our present research seeks to reveal, both numerically and experimentally, the natural convective flow and temperature characteristics in a single-phase, closed thermosyphon with an adiabatic zone.

☆ This paper is a revised and expanded version of a paper presented at CHT'01, the Second International Symposium on Advances in Computational Heat Transfer (Palm Cove, Qld., Australia, 20–25 May 2001), the proceedings of which were published by Begell House, Inc.

* Corresponding author. Tel.: +81-6-6368-1121; fax: +81-6-6388-8785.

E-mail address: ishihara@kansai-u.ac.jp (I. Ishihara).

0142-727X/02/$ - see front matter
PII: S0142-727X(02)00184-4

Nomenclature

c	heat capacity	W	width of enclosure
D	distance between heat transfer surfaces	x	horizontal coordinate normal to heat transfer surface
g	gravitational acceleration		
H	height of enclosure	y	horizontal coordinate parallel to heat transfer surface
p	pressure		
Pr	Prandtl number	z	vertical coordinate
Ra	Rayleigh number		
T	temperature		
T_C	cooling surface temperature	*Greeks*	
T_H	heating surface temperature	β	volumetric expansion
u	velocity in x direction	λ	thermal conductivity
v	velocity in y direction	μ	dynamic viscosity
w	velocity in z direction	ρ	density

The enclosure employed as rectangular thermosyphon model was constructed of transparent plexi-glass plates that allowed visualization of the fluid flow and temperature fields. Two symmetrical vertical plates of 100 mm height and 100 mm width function as the heat transfer surfaces, each comprising both a cooling and a heating zone, while the others provide adiabatic walls. The two heat transfer surfaces comprise three elevations, each of equal height, the top and bottom thirds of each surface functioning respectively as isothermally cooling and heating zones, while their respective intermediate sections act as adiabatic zones.

The temperature difference between the heating and the cooling surfaces, and the distance, D, between the heat transfer surfaces, are the relevant variable parameters. Temperature and velocity fields are visualized by means of thermo-sensitive liquid crystal powders, and photographed by means of the light sheet method.

2. Experimental apparatus and procedure

The test section and its coordinate system are illustrated in Fig. 1. The transport properties of the silicon oil used as a working fluid are listed in Table 1. The test section consists of transparent plexi-glass plates of 2 mm thickness for heat transfer surfaces, and 10 mm thickness for the other walls, and has $H = 100$ mm height, $W = 100$ mm width, while the distance, D, between the two heat transfer surfaces was, on the inside, given the variations of 5, 25 and 50 mm.

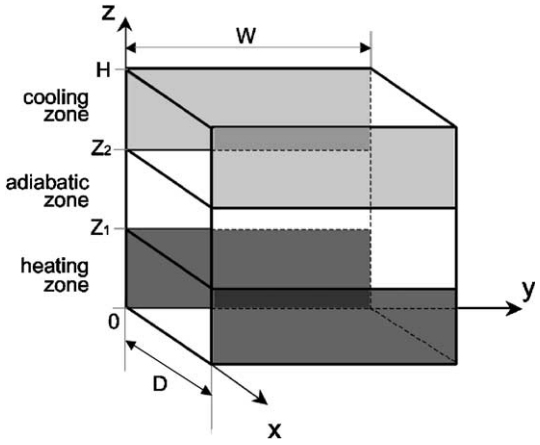

Fig. 1. Schematic of test section and coordinate system.

The heat transfer surfaces are separated into three elevation zones of equal height. The top third of each surface forms a cooling zone, while its bottom third is the heating zone. The heat transfer surfaces are maintained at constant temperatures by heating and cooling the exteriors of these surfaces with temperature-regulated water.

The intermediate section of the heat transfer surfaces acts as an adiabatic zone. There are narrow spaces filled with air at the boundaries of these adiabatic zones, provided to ensure thermal insulation. After being entirely filled with silicon oil, the chosen working fluid, this test section is placed in a large box that is isolated thermally from the environment, and in which the

Table 1
Transport properties of working fluid

Working fluid	Kinematic viscosity (m^2/s)	Density (kg/m^3)	Specific heat capacity (J/kg K)	Thermal conductivity (W/mK)	Coefficient of volumetric expansion (K^{-1})	Pr (–)
Silicon oil	2.0×10^{-5}	948	1.51×10^3	0.146	1.01×10^{-3}	212

ambient air temperature around the test section is kept a constant temperature of 19.5 °C. This is effected through use of operating heat exchangers with circulation fans that are controlled by a circulating water flow drawn from a temperature regulated bath.

Experiments were conducted as follows: The test section is filled up with the working fluid, which has been pre-mixed with thermo-sensitive liquid crystal powders (RW-2024), employed in order to visualize both the temperature and the flow fields. As the concentration of the crystal powders is about 0.1 wt.%, no effect on the properties of the fluid needs be considered.

At the beginning of each experiment, the temperature of the fluid in the test section is controlled and kept constant at 19.5 °C by both heating and cooling of the heat transfer surfaces, 19.5 °C being the middle value of the temperature zone presented by the coloration range of the thermo-sensitive liquid crystal powders used. Next, the temperature difference, ΔT, between the heating and cooling surfaces is set in a range between 0.5 and 4 K, centered on the middle temperature of the coloration range. More than an hour after reaching a steady condition, the temperature and velocity fields in an arbitrary plane (y–z or z–x plane) are visualized by illuminating the working fluid with a Xe-light sheet, and are then photographed using a still camera and an exposure of 8 s.

3. Numerical calculation

Laminar natural convection within the enclosure was analyzed by solving a set of governing equations for a three-dimensional steady state; these are shown below, together with the relevant boundary conditions. The Boussinesq approximation has been assumed to be applicable.

$$\frac{\partial u}{\partial x}+\frac{\partial v}{\partial y}+\frac{\partial w}{\partial z}=0$$

$$\rho\left(u\frac{\partial u}{\partial x}+v\frac{\partial u}{\partial y}+w\frac{\partial u}{\partial z}\right)=-\frac{\partial p}{\partial x}+\mu\left(\frac{\partial^2 u}{\partial x^2}+\frac{\partial^2 u}{\partial y^2}+\frac{\partial^2 u}{\partial z^2}\right)$$

$$\rho\left(u\frac{\partial v}{\partial x}+v\frac{\partial v}{\partial y}+w\frac{\partial v}{\partial z}\right)=-\frac{\partial p}{\partial y}+\mu\left(\frac{\partial^2 v}{\partial x^2}+\frac{\partial^2 v}{\partial y^2}+\frac{\partial^2 v}{\partial z^2}\right)$$

$$\rho\left(u\frac{\partial w}{\partial x}+v\frac{\partial w}{\partial y}+w\frac{\partial w}{\partial z}\right)=-\frac{\partial p}{\partial z}+\mu\left(\frac{\partial^2 w}{\partial x^2}+\frac{\partial^2 w}{\partial y^2}+\frac{\partial^2 w}{\partial z^2}\right)+\rho g\beta(T-T_C)$$

$$\rho c\left(u\frac{\partial T}{\partial x}+v\frac{\partial T}{\partial y}+w\frac{\partial T}{\partial z}\right)=\lambda\left(\frac{\partial^2 T}{\partial x^2}+\frac{\partial^2 T}{\partial y^2}+\frac{\partial^2 T}{\partial z^2}\right)$$

Boundary conditions: $T=T_H$ at $x=0$ and D, $0\leqslant y\leqslant W$, $0\leqslant z\leqslant z_1$, $T=T_C$ at $x=0$ and D, $0\leqslant y\leqslant W$, $z_2\leqslant z\leqslant H$ and all of the other parts of the surfaces are adiabatic. No slip condition is applied on any of the surfaces.

Numerical calculation was performed by means of SIMPLE scheme; the procedure chosen is as follows; initially, the temperature of the fluid and the adiabatic wall surfaces are kept in the middle of ΔT, and the fluid is at rest. When setting the temperature difference, ΔT, the calculation starts and is iterated. If the deviation of velocity, temperature and pressure remained within 1% during no more than 20,000 iterations, a steady state is regarded as having been attained, and, if not, it is judged that a converged solution is not obtained.

In this paper, the calculated results will be illustrated for a small $D=5$ mm, $\Delta T=1.0$ K and for a large $D=50$ mm, $\Delta T=2.0$ K, and the Rayleigh number, Ra, with a reference length (z_2-z_1) is 1.95×10^5, 3.89×10^5 and the Prandtl number is 212 in these conditions.

The number of grids for calculation was 102 in both y and z directions, and a 17-grid was applied in x direction for $D=5$ mm, a 32-grid for $D=25$ mm and a 52-grid for $D=50$ mm. In order to examine the dependence of number of grids on calculated results, the number of grids in x direction alone was changed to 27 and 32 for $D=25$ mm, and 17 and 32 for $D=5$ mm. No variation in the results obtained at the monitoring point ($D/2$, $W/2$, $H/2$) was found at the maximum number of grids within the above accuracy.

4. Results and discussion

Working from the numerical calculations and the observations of the fluid flow, a flow pattern map is drawn, as shown in Fig. 2, where numerical calculations give a regime of steady flow. With a very small D, such as 5 mm, a small ΔT allows a steady, quasi-two-dimensional flow. With a D larger than 25 mm, a steady, three-dimensional flow results for a ΔT larger than 2.0 K. With an intermediate range of D, of between 5 and 25

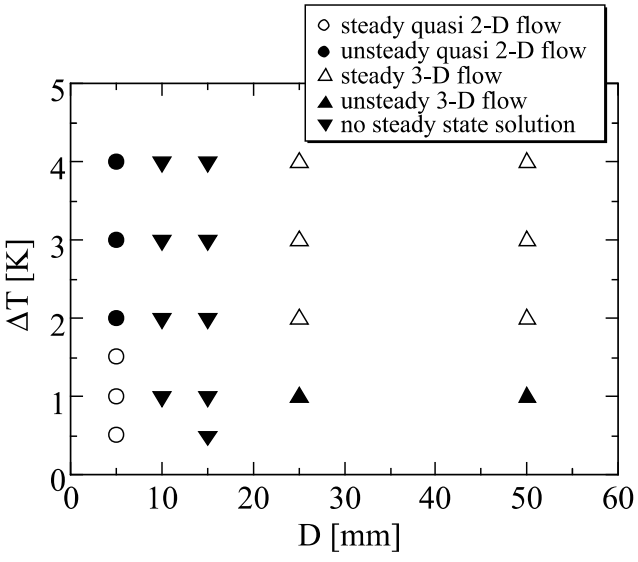

Fig. 2. Flow pattern map.

mm, a steady flow is not found for the entire range of ΔT from the calculation; and an unsteady, three-dimensional flow occurs for a large D and $\Delta T = 1$ K. This suggests that, in the case of a wide D, a relatively large buoyancy is needed, in order that the fluid is driven steadily. The experimental and numerical results revealed that the steady, quasi-two-dimensional flow patterns only occur where both D and ΔT are small, and a steady, three-dimensional flow appears with a combination of a large D and a relatively large ΔT. The steady flows will next be discussed in detail.

4.1. Steady, quasi-two-dimensional flow

Fig. 3(a) presents a photograph of a steady, quasi-two-dimensional temperature profile and flow pattern for $D = 5$ mm and $\Delta T = 1.0$ K. This photograph was taken in a y–z plane, very close to the heat transfer surface at $x \cong 4$ mm. In this photograph, the lower, green-colored region indicates a higher temperature, while the upper, red-colored region indicates a lower.

Many streaklines, traced by the thermo-sensitive crystal powders, are to be seen; these reveal four large flows, circulating symmetrically with respect to the almost central line, $y = 50$ mm. These circulating flows are formed, on one hand, by two cooled, downward flows around $y = 25$ and 75 mm, which penetrate into the heating zone, and, on the other, three heated, upward flows at the y positions close to the center and both sidewalls. The downward flows are heated in the heating zone, then to turn upward after separating horizontally, in mutually opposed directions.

The numerical results obtained for the same conditions as those in this experiment are presented in Fig. 3(b). Although the flow pattern is a mirror image reversed on a horizontal axis of that gained in the experiment, in all other respects the pattern thus derived closely resembles that observed in the experiment; moreover, the experimental value of vertical velocity obtained from the length of the powder traces coincides with the velocity as calculated.

A very similar steady, two-dimensional flow was also found in the same size of enclosure under the condition of a small D and a small ΔT, in which only one vertical surface functioned as heat transfer surface, Ishihara et al. (2000).

When the ΔT is further increased, the buoyancy predominates over the viscous force acting on the working fluid, so that the flow pattern changes, and flow-fluctuation periodically appears.

4.2. Steady, three-dimensional flow

Fig. 4 shows photographs of temperature profiles and streaklines in the y–z and z–x planes for $D = 50$ mm and $\Delta T = 2.0$ K. Fig. 5 is a representation of the numerical results for the same condition as that of Fig. 4. Fig. 4-1 presents a temperature profile in the y–z plane very close to the heat transfer surface.

This shows a flow pattern consisting mainly of vertical, upward flows in the lower region, and downward flows in the upper region of the y–z plane. These flows create a counter-flow of the same velocity, and flows and counter-flows then meet and form a fork-like ''interdegitative flow'' at the mid-plane of z direction. As a result, a cyclically wavy pattern of temperature appears.

Fig. 4-2 displays both the temperature profile and the flow pattern at the cross-sections (z–x planes) passing through the bottom in (a), and top in (b), of the temperature wave. To make the flow characteristics more

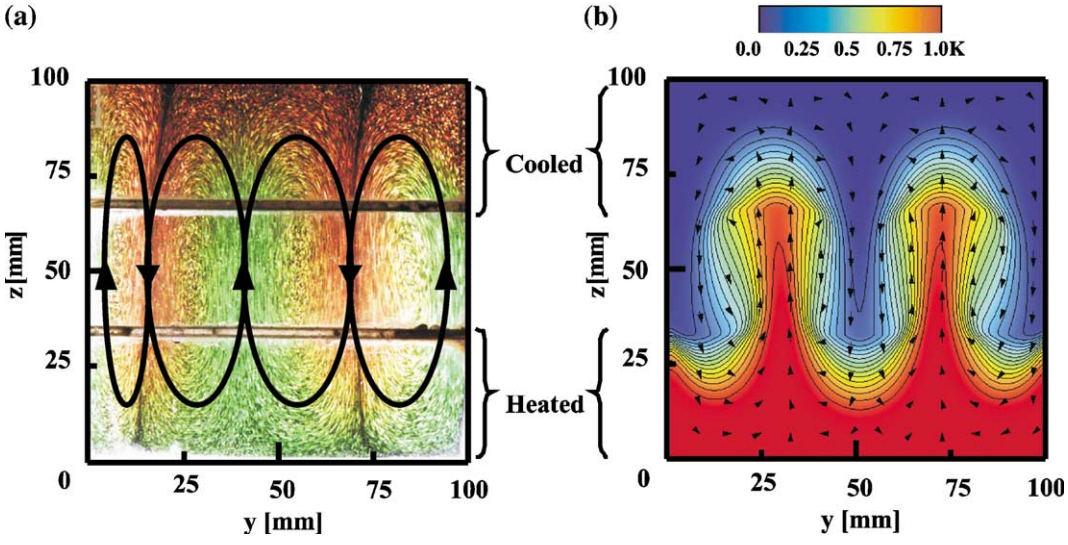

Fig. 3. (a) Temperature profiles and streamlines at $x \cong 4$ mm in y–z plane for $D = 5$ mm and $\Delta T = 1.0$ K. (b) Calculated temperature profiles, isotherms and velocity vectors at $x = 4$ mm in y–z plane for $D = 5$ mm and $\Delta T = 1.0$ K.

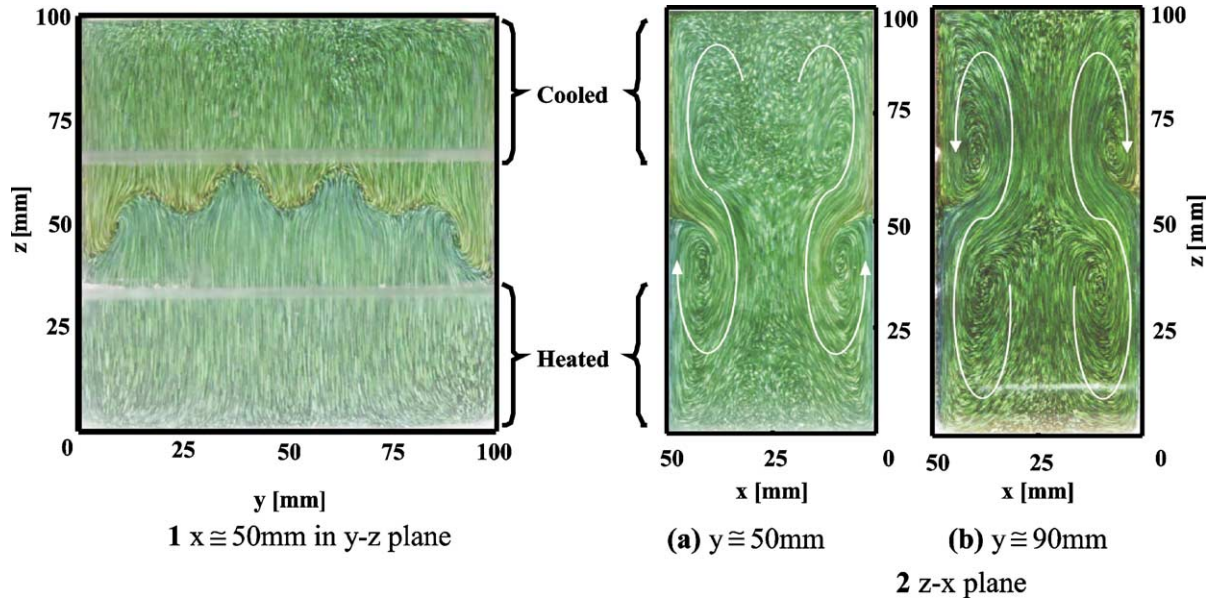

Fig. 4. Temperature profiles and streak lines for $D = 50$ mm and $\Delta T = 2.0$ K; (1) $x \cong 50$ mm in y–z plane; (2) z–x plane: (a) $y \cong 50$ mm, (b) $y \cong 90$ mm.

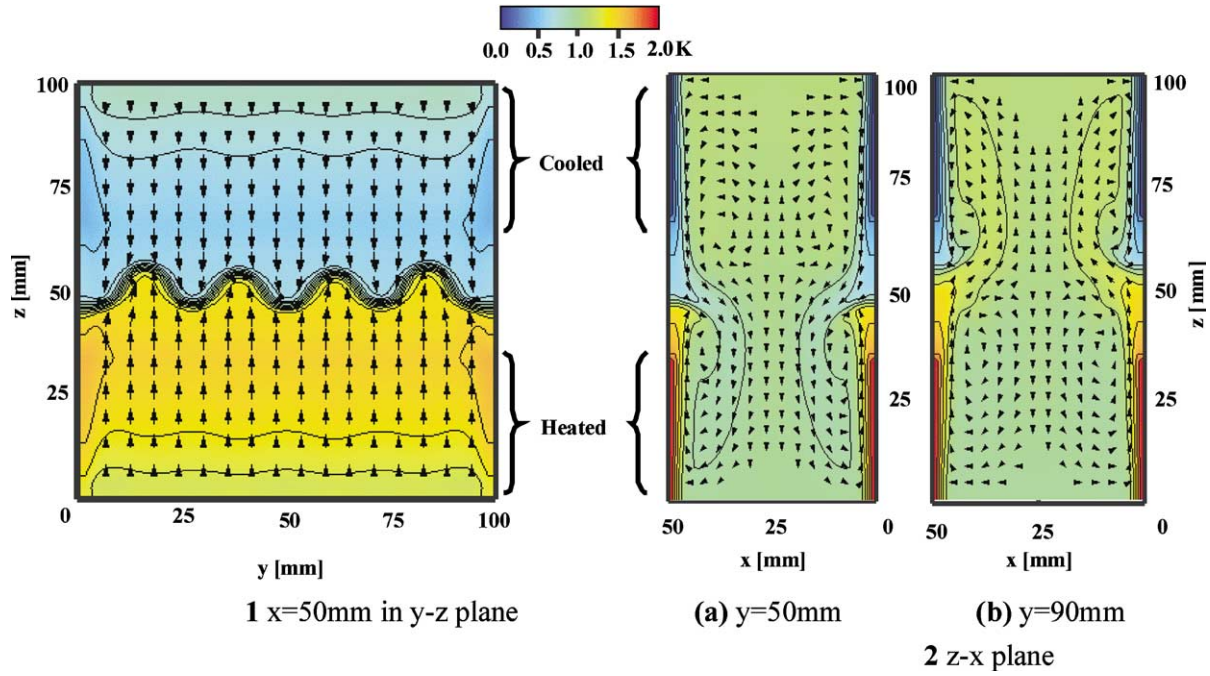

Fig. 5. Temperature profiles, isotherms and velocity vectors from numerical results for $D = 50$ mm and $\Delta T = 2.0$ K; (1) $x = 50$ mm in y–z plane; (2) z–x plane: (a) $y = 50$ mm, (b) $y = 90$ mm.

clearly visible, representative streamlines have been superimposed. The temperature and velocity profiles in Fig. 4-2(a) and (b) are mutually symmetrical with regard respectively to the vertical line at $x = 25$ mm and the horizontal line at $z = 50$ mm.

The boundary layer flows along both cooling and heating surfaces meet near the mid-plane, at $z = 50$ mm, and penetrate into their respective opposite zones.

In Fig. 4-2(a), the cooled flow descends, is distorted towards the central vertical axis in the intermediate zone, so as to avoid collision with the upward flow, and then penetrates into the heating zone. After that, it joins the upward flow and rises along the heating surface. When approaching the mid-plane, this heated upward flow turns in y direction, separates from the heating surface, and then enters the cooling zone, thus tracing

figures-of-eight, one the mirror image of the other. Fig. 4-2(b) likewise displays a pair of similar, figure-of-eight flow patterns, save for the fact that the flow directions are the reverse of those in Fig. 4-2(a).

The two symmetrical, figure-of-eight flow patterns shown in Fig. 4-2(a) and (b) combine to make one pair; which means that four pairs, i.e. eight figure-of-eight streamlines, range in parallel in the enclosure. And this is the structure of the steady, three-dimensional flow.

As the ΔT increases, buoyancy as the driving force of convection flow increases in strength, with the result that the flow velocity is accelerated; and this increases the number of figure-of-eight flow-streams. For instance, when $\Delta T = 2.0$ K, as shown in Fig. 4, the number of pairs of figure-of-eight streams is four; and with an increase of ΔT up to 4.0 K, this number increases to six, while the effect of distance, D, on the number is very small. The contribution of D to natural convection is to stabilize the fluid flow.

Numerical results calculated for the same conditions as those for the experiment recorded in Fig. 4 are, in Fig. 5, represented as temperature profiles, isotherms and flow patterns in planes corresponding to those in Fig. 4. Fig. 5 illustrates detailed features of the flow and temperature distributions mentioned above, and comparison with the those of the experiment reveals how very well the numerical results simulate the real phenomena involved.

Fig. 6 displays the calculated temperature patterns and velocity vectors in x–y planes for $z = 40$–60 mm in the intermediate zone. In all x–y planes it will be seen that both temperature and velocities of u and v are mirror images distributed symmetrical on the axes represented by the centerlines of x and y directions, and that temperature distributions in both upward and downward flow regions undergo a perfect mutual interchange with regard to $z = 50$ mm. The yellow and blue heart-shaped portions indicate respectively the area of upward and downward streams and correspond to the top and bottom of the wavy temperature profile in Fig. 5-1.

Above have been described the velocity profiles and the structure of the steady, three-dimensional flow. In order to observe these globally, in Fig. 7 a number of the streamlines obtained by calculation have been represented three-dimensionally. The result illustrates that eight figure-of-eight flow streamlines are ranged side by side. From this, the structure of a steady, three-dimensional flow can be well understood.

In addition, Fig. 8 shows in three dimensions the distributions of the vertical velocity in the mid-plane. The upward flow forms 8 peaks, and the downward 10. These positive and negative peaks are positioned alternately and are of symmetry with regard to the vertical planes at $x = 25$ and at $y = 50$ mm respectively. This

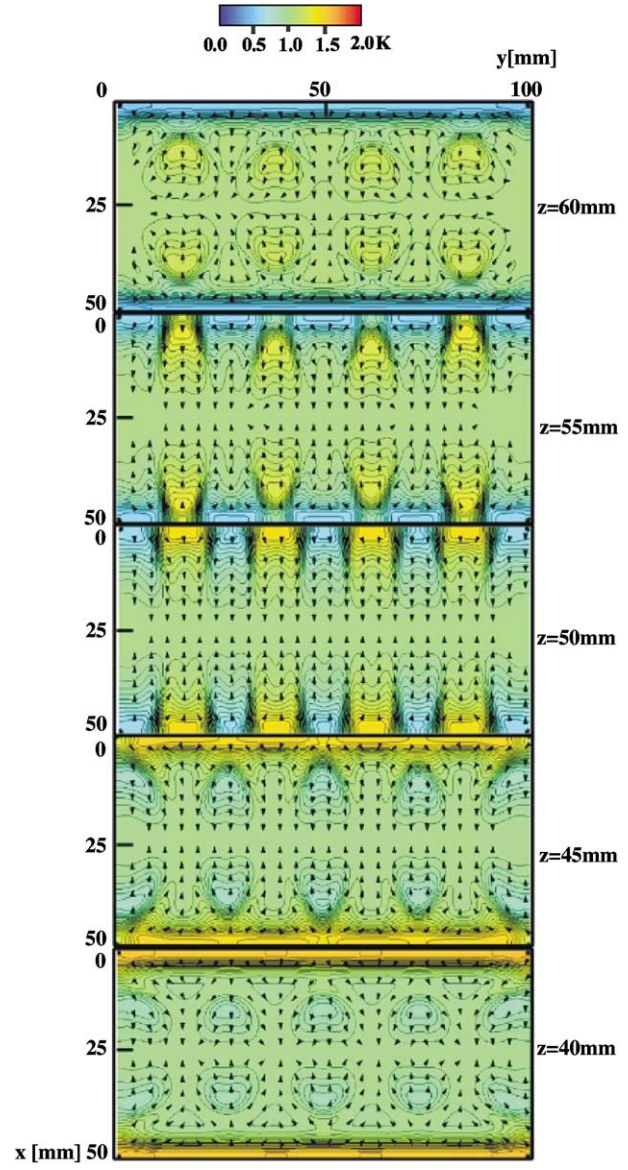

Fig. 6. Temperature distributions, isotherms and velocity vectors in x–y planes from calculation for $D = 50$ mm and $\Delta T = 2.0$ K.

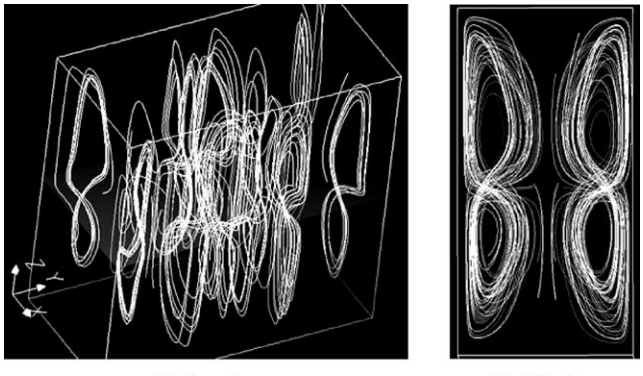

Fig. 7. Structure of three-dimensional steady flow from calculation for $D = 50$ mm and $\Delta T = 2.0$ K. (a) Overview, (b) side view.

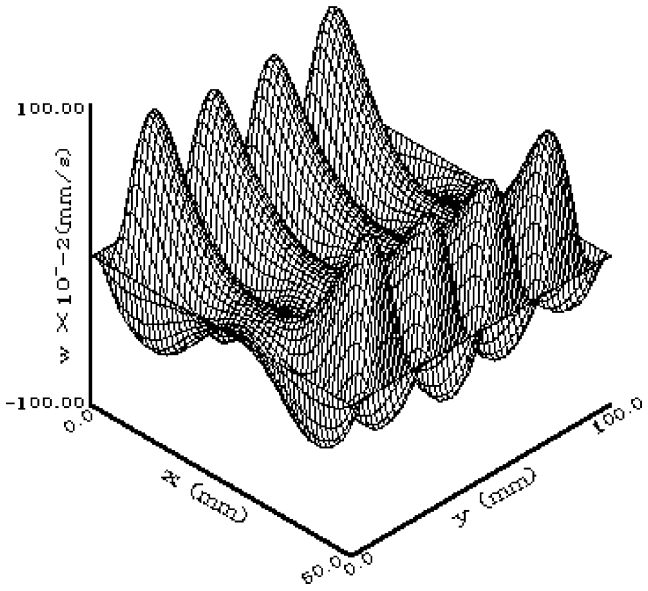

Fig. 8. Velocity profile w in z-direction in the center plane for $D = 50$ mm and $\Delta T = 2.0$ K.

figure explains very well how the counter-flows branch in the central horizontal plane. Such branch flow is what results in a steady, three-dimensional flow.

5. Conclusions

Numerical and experimental studies of natural convection in a single phase, closed thermosyphon were carried out using a vertical, rectangular enclosure model, in which two symmetrically-placed vertical plates played the role of heat transfer surfaces. By changing the distance, D, or the temperature difference, ΔT, it has proved possible to classify the natural convection flow observed into three patterns: a steady, quasi-two-dimensional flow that is found for both a small D and a small ΔT, a steady, three-dimensional flow that appears for a large D and a large ΔT, and an unsteady flow.

The steady, quasi-two-dimensional flow consists of four large flows circulating symmetrically with respect to the centerline $y = 50$ mm. The steady, three-dimensional flow is composed of figure-of-eight streamlines, and the number of these stream lines increases with increase in ΔT.

Numerical calculation simulates well the real phenomena of the steady flow, and two types of steady flow structure have been revealed in detail through both experiment and calculation.

References

Bayley, F.J., Lock, G.S.H., 1965. Heat transfer characteristics of the closed thermosyphon. J. Heat Transfer 87, 30–40.

Japikse, D., 1973. Advances in thermosyphon technology. In: Adv. Heat Transfer 9. Academic Press, London, p. 47.

Mallinson, G.D., Graham, A.D., de Vahl Davis, G., 1981. Three-dimensional flow in a closed thermosyphon. J. Fluid Mech. 109, 259–275.

Ishihara, I., Matsumoto, R., Seno, A., 2000. Natural convection in a vertical rectangular enclosure with localizing heating and cooling zones. Heat Mass Transfer 36, 467–472.